ACS Catalysis

Research Article

pubs.acs.org/acscatalysis

Oxygen Reduction Catalyzed by Platinum Nanoparticles Supported on Graphene Quantum Dots

Guoqiang He,† Yang Song,† Ke Liu,† Andrew Walter, Sophie Chen, and Shaowei Chen*

Department of Chemistry and Biochemistry, University of California, 1156 High Street, Santa Cruz, California 95064, United States

Supporting Information

ABSTRACT: Nanosized graphene quantum dots were prepared by acid etching of carbon fibers and used as effective substrate supports for platinum nanoparticles which were synthesized by thermolytic reduction of platinum(II) chloride in ethylene glycol. Transmission electron microscopic measurements showed that the resulting nanocomposite (Pt/G) particles exhibited an average diameter of 2.79 ± 0.38 nm, with clearly defined lattice fringes of 0.23 nm that might be assigned to the interlayer spacing of the (111) crystal planes of *fcc* Pt. In addition, the Pt nanoparticles were found to be wrapped with a low-contrast halo that likely arose from the poorly crystalline graphene quantum dots. X-ray diffraction studies confirmed the composite nature of the Pt/G nanoparticles, and the average size of the crystal domains of the Pt/G nanoparticles was found to be close to the nanoparticle physical dimensions, whereas for commercial Pt/C nanoparticles the size of the crystal domains was only half that of the nanoparticle diameter. XPS measurements showed the formation of metallic platinum along with sp^2 and oxygenated carbons in the nanocomposite nanoparticles. Significantly, in comparison with commercial Pt/C catalysts, the Pt/G nanocomposites showed markedly enhanced catalytic activity in oxygen reduction reactions, with an onset potential of +1.05 V that was 70 mV more positive than that of Pt/C, and a specific activity that was almost nine times higher. These results were ascribed to the abundant structural defects of the nanosized graphene quantum dots that manipulated the dissociative adsorption of oxygen and the binding of reaction intermediates O* and HO* on platinum surfaces.

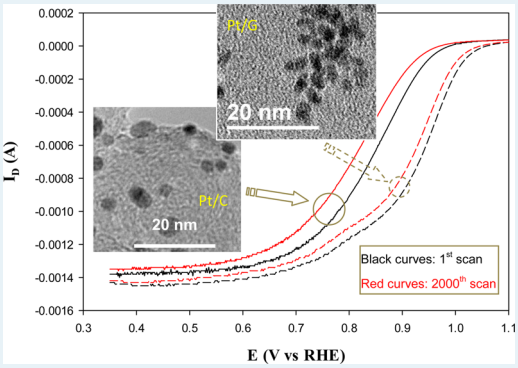

KEYWORDS: *graphene quantum dot, platinum nanoparticle, oxygen reduction, defect, X-ray diffraction, XPS, Tafel plot*

INTRODUCTION

Precious metals have been used extensively as effective cathode catalysts for oxygen reduction in proton exchange membrane fuel cells. Typically these materials are dispersed as nanosized particles on supporting substrates of high surface areas to enhance accessibility and to reduce costs. In these, it has been found that the electronic interactions between the metal nanoparticles and the supporting substrates might also play a significant role in determining the electrocatalytic activity as a result of the manipulation of the electronic energy of the metal nanoparticles and hence the interactions with oxygen.[1−4] In both industrial and academic research, carbon-based materials are one of the most commonly used supporting substrates, such as carbon black, carbon nanotubes, and graphene sheets.[5−9] This is largely due to their low cost, high surface area, high conductivity, and high chemical inertness that may facilitate electron-transfer reactions at the electrode surface and hence improve catalyst stability and durability.

Among these, while a relatively new addition, graphene has attracted particular research interest in fuel cell electrocatalysis. In fact, a number of studies have been reported recently in the literature where graphene sheets are used as a support for the nanoparticle catalysts in oxygen reduction.[10,11] For instance, platinum nanoparticles (from 2.2 to 5.6 nm in dia.) supported on reduced graphene oxides (Pt/RGO) have been prepared by using perfluorosulfonic acid as the functionalization and anchoring reagent.[12] The catalytic performance in oxygen reduction was found to be enhanced by hydrogen heat treatment, which was ascribed to the bifunctional effects of both improved graphitization and the oxygenated groups on the catalytic activity and stabilization of the metal nanoparticles. In another study,[13] graphene-supported platinum nanoparticle composites were prepared by a chemical co-reduction method. The platinum nanoparticles were between 3.30 and 4.45 nm in diameter and exhibited apparent electrocatalytic activity in oxygen reduction. Furthermore, a composite catalyst has also been prepared by using graphene-supported platinum nanoparticles (average diameter 3.4 nm) impregnated with ionic liquid that exhibited enhanced electrocatalytic activity and excellent methanol tolerance for oxygen reduction because of increasing oxygen-philicity and methanol-phobicity.[14]

In these early studies, the graphene sheets are generally produced from bulk graphite by the Hummers method through chemical oxidation and exfoliation with strong acids and

Received: February 13, 2013
Revised: March 18, 2013
Published: March 19, 2013

oxidizing reagents.[15] The obtained graphene sheets mostly exhibit irregular shapes and a large size dispersity (ranging from nanoscale to micrometer-scale), and are prone to folding and wrinkling because of the strong $\pi-\pi$ interactions, thus compromising the even dispersion and ready accessibility of the metal nanoparticle catalysts.[16−18] To overcome such technical challenges, a recent study showed that by inserting carbon black particles between the RGO sheets, stacking of RGO might be minimized, hence promoting oxygen diffusion through the RGO sheets and enhancing the electrocatalytic performance of graphene-supported Pt nanoparticles (5 nm in dia.).[5] Such issues can also be resolved by using nanosized graphene sheets.[19−21] Recently, an effective protocol was reported for the preparation of nanometer-sized graphene quantum dots (GQDs) where the stacked submicrometer domains of traditional pitch-based carbon fibers were broken down by acid treatments and chemical exfoliation.[21] The size of the resulting GQDs was found to be within the range of 1 to 4 nm with 1 to 3 layers in thickness. Because of their large surface-volume ratio, such GQDs are anticipated to exhibit abundant structural defects, which may be exploited to promote charge transfer from platinum to oxygen as well as to manipulate the binding of reaction intermediates on the Pt surface, as suggested in a recent theoretical study.[22] This is the primary motivation of the present study.

In this study, we adopted the literature procedure to prepare GQDs from carbon fibers[21] and then used them as supporting substrates for platinum nanoparticles. The electrocatalytic activity of the resulting nanocomposites (Pt/G) in oxygen reduction was then examined in acid electrolyte solutions, using commercial Pt/C catalysts as a benchmark material for comparative study. Voltammetric measurements showed that while oxygen was effectively reduced to water at both nanoparticle catalysts, the Pt/G nanocomposites exhibited a markedly enhanced electrocatalytic performance with a more positive onset potential, higher specific activity as well as stability, as compared to commercial Pt/C. The results were accounted for by the intimate electronic interactions between the nanosized GQDs and the Pt nanoparticles that manipulated the dissociative adsorption of oxygen and the binding of reaction intermediates on the Pt surface.

EXPERIMENTAL SECTION

Chemicals. Platinum(II) chloride ($PtCl_2$, 98%, Sigma-Aldrich), pitch carbon fibers (Fiber Glast Development Corporation), sodium carbonate (Na_2CO_3, ≥99.5%, Sigma-Aldrich), ammonia (28 wt % in water, Acros), perchloric acid ($HClO_4$, 70 wt %, ACROS), sulfuric acid (H_2SO_4, Fisher Scientific), nitric acid (HNO_3, Fisher Scientific), high-purity O_2 (99.993%, Airgas), and a commercial Pt/C catalyst (20 wt.%, Johnson Matthey) were used as received. Water was supplied by a Barnstead Nanopure water system (18.3 MΩ·cm).

Graphene Quantum Dots (GQDs). The GQDs were prepared by following a literature procedure.[21] In brief, 0.30 g of carbon fibers was added into a mixture of concentrated H_2SO_4 (60 mL) and HNO_3 (20 mL). The solution was sonicated for 2 h and stirred for 24 h at 120 °C. The mixture was then cooled and diluted with Nanopure water (800 mL) with the pH adjusted to about 8 by Na_2CO_3. The solution was then dialyzed in a dialysis bag (cutoff molecular weight 2000 Da) for 3 d, affording purified GQDs, which then underwent spectroscopic characterizations (Supporting Information, Figures S1 and S2). These GQDs were then used as supporting substrates for platinum nanoparticles, as detailed below.

GQD-Supported Platinum Nanoparticles (Pt/G). In a typical reaction, $PtCl_2$ (26.6 mg, 0.1 mmol) was dissolved in 2 mL of hydrochloric acid under heating. The solution was then condensed to about 1 mL and added into 100 mL of ethylene glycol, along with 80 mg of GQDs prepared above under magnetic stirring. The pH was adjusted to 10 by concentrated ammonia, and the mixture was heated at 165 °C for 30 min, where black precipitates appeared in the flask as a result of thermolytic reduction of Pt(II) by ethylene glycol to form GQDs-supported platinum (Pt/G) nanoparticles. The precipitates were collected, washed extensively with Nanopure water, and dried in a vacuum oven at 80 °C for 12 h. The product contained 20 wt % of Pt, similar to that of commercial Pt/C catalysts.

Structural Characterizations. High-resolution transmission electron microscopic (TEM) studies were carried out with a JEOL JEM-2010 TEM microscope operated at 200 kV. The crystalline properties of the nanoparticle catalysts were evaluated by powder X-ray diffraction (XRD) measurements with a Rigaku Mini-flex Powder Diffractometer using Cu−Kα radiation with a Ni filter (λ = 0.154059 nm at 30 kV and 15 mA). X-ray photoelectron spectra (XPS) were recorded with a PHI 5400 XPS instrument equipped with an Al Kα source operated at 350 W and at 10^{-9} Torr. The spectra were charge-referenced to the Au4f $_{7/2}$ peak (83.8 eV) of sputtered gold. Dynamic light scattering (DLS) measurements were carried out with a Wyatt Protein Solution *Dynapro* Temperature Controlled Microsampler.

Electrochemistry. Electrochemical measurements were carried out with a CHI440 electrochemical workstation using a standard three-electrode cell with separate anode and cathode compartments. A platinum foil and a reversible hydrogen electrode (RHE) were used as the counter and reference electrode, respectively. The working electrode was a glassy-carbon disk electrode (diameter 5.61 mm) of a rotating ring-disk electrode (RRDE, with a collection efficiency of 37%) from Pine Instrument, Inc.[23] The RRDE was prepared according to a procedure proposed by Gloaguen et al.[24] In a typical experiment, Pt/G was mixed under ultrasound with a Nafion solution (5 wt %, Fluka) to form a well dispersed catalyst "ink". A calculated amount of the catalyst inks was then dropcast onto the polished glassy carbon disk electrode. The commercial Pt/C was loaded onto the electrode in a similar fashion. The mass loading of Pt on both electrodes was kept at about 12.1 μg.

Prior to electrochemical tests of oxygen reduction, the catalyst films on the glassy-carbon electrode were electrochemically pretreated in a nitrogen-saturated 0.1 M $HClO_4$ solution by potential cycling at 200 mV/s between +0.05 V and +1.10 V until a steady voltammogram was observed. The electrocatalytic activity for oxygen reduction was then evaluated in an O_2-saturated 0.1 M $HClO_4$ solution by using a rotating (ring-)disk electrode system (Pine Instrument Inc.) at a rotation rate of 100 rpm to 2500 rpm. The electrode potential was swept from +0.05 V to +1.10 V at 5 mV/s, and the solution ohmic drop (i.e., IR drop) was electronically compensated.

RESULTS AND DISCUSSION

Note that from DLS measurements the average hydrodynamic diameter of the as-produced GQDs was estimated to be 14.5 ± 3.9 nm; and AFM topographic analysis indicated that the thickness of the graphene quantum dots ranged from 0.5 to 2.0

dx.doi.org/10.1021/cs400114s | ACS Catal. 2013, 3, 831−838

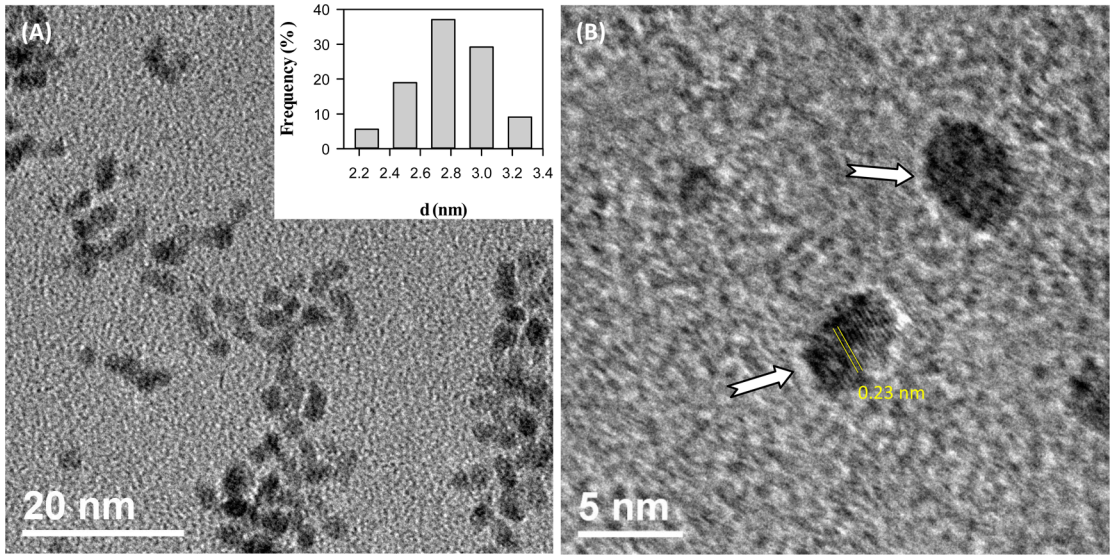

Figure 1. Representative TEM micrographs of GQD-supported Pt nanoparticles. Scale bar is 20 nm in panel (A) and 5 nm in panel (B). Inset in panel (A) shows the nanoparticle core size histogram. Yellow lines in panel (B) highlight the lattice fringes, and white arrows indicate the halos surrounding the Pt nanoparticles.

nm, corresponding to one to four graphene (oxide) layers in the samples, consistent with TEM measurements (Supporting Information, Figure S1). These GQDs were then used to prepare Pt/G hybrid nanoparticles. Figure 1 shows two representative TEM micrographs of the Pt/G nanoparticles. In panel (A), it can be seen that the nanoparticles were dispersed rather homogeneously on the TEM grid, with the majority of the nanoparticles in the narrow range of 2.5 to 3.0 nm in diameter, as manifested in the core size histogram in the figure inset. In addition, statistical analysis shows that the average nanoparticle core diameter was 2.79 ± 0.38 nm, slightly smaller than that of commercial Pt/C (3.30 ± 0.42 nm).[23] Furthermore, from high-resolution TEM studies in panel (B), clearly defined lattice fringes can be identified, as highlighted by yellow lines, with a spacing of 0.23 nm. These are consistent with the (111) crystalline planes of *fcc* Pt.[23] In addition, one may see that the Pt nanoparticles were surrounded by a low-contrast halo, as indicated by white arrows, which might be ascribed to the GQDs that exhibited low crystallinity and low electron-density contrast. These results suggest the formation of an intimate composite structure in the Pt/G nanoparticles.

The composite nature of the Pt/G nanoparticles was further manifested in XRD measurements. From Figure 2, one can see that the nanoparticles (red curve) exhibited three well-defined diffraction peaks at $2\theta = 39.85°$, 46.23°, and 67.60° that may be assigned to the (111), (200), and (220) crystalline planes of *fcc* Pt, respectively. Additionally, the Pt/G nanoparticles also displayed two broad diffraction peaks centered at $2\theta \approx 25.80°$ and 22.67°, corresponding to a lattice spacing of 0.345 and 0.392 nm, respectively. Whereas both may be assigned to the graphite (002) planes, the somewhat larger value of the latter suggests lattice expansion as a result of the formation of oxygen-containing groups during the chemical oxidation and exfoliation of the carbon fibers.[21] Additionally, the broad appearance of these peaks signifies the low crystallinity of the resulting GQDs, consistent with the results in TEM measurements presented in Figure 1 (B). Such diffraction features can also be clearly identified with the commercial Pt/C sample

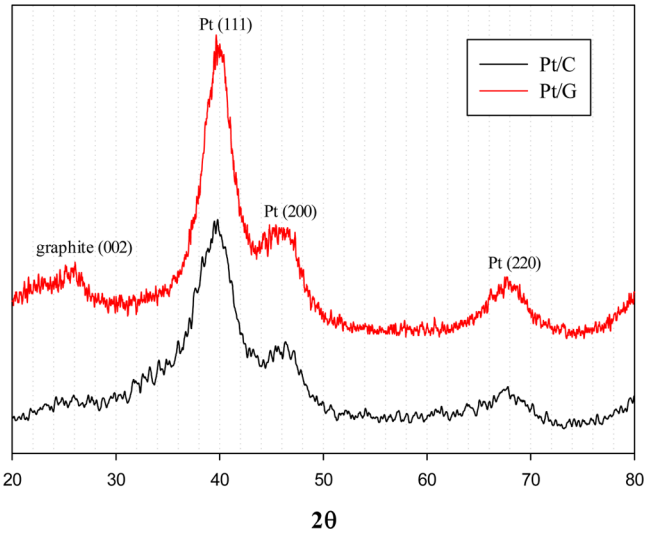

Figure 2. XRD patterns of the Pt/G and Pt/C nanoparticles.

(black curve), except that the graphite diffraction peak was rather weak and ill-defined.

Furthermore, the average size (τ) of the crystalline domains of the Pt nanoparticles can be estimated by the Debye–Scherrer equation,[25] $\tau = K\lambda/\beta \cos\theta$, where K is a dimensionless shape factor with a value of ~0.9, λ is the X-ray wavelength (1.54059 Å for Cu–Kα), and β is the full width at half-maximum (fwhm) of a selected diffraction peak. Therefore, based on the fwhm of the Pt(111) diffraction peaks, the average size of the nanoparticle crystalline domains was estimated to be 1.54 nm for Pt/C and 2.62 nm for Pt/G. The fact that the size of the crystalline domains of the Pt/G nanoparticles was close to their geometrical diameter as determined by TEM measurements (Figure 1) signifies that the nanoparticles were likely of single crystal structures, in agreement with the clearly defined lattice fringes throughout the entire nanoparticles. In contrast, the size of the crystalline domains of the Pt/C nanoparticles was only half of the physical dimensions,

dx.doi.org/10.1021/cs400114s | *ACS Catal.* 2013, 3, 831–838

suggesting a polycrystalline nature of the platinum nanoparticles in the commercial sample.

The formation of a platinum-graphene nanocomposite in Pt/G particles was also evidenced in XPS measurements. Figure 3

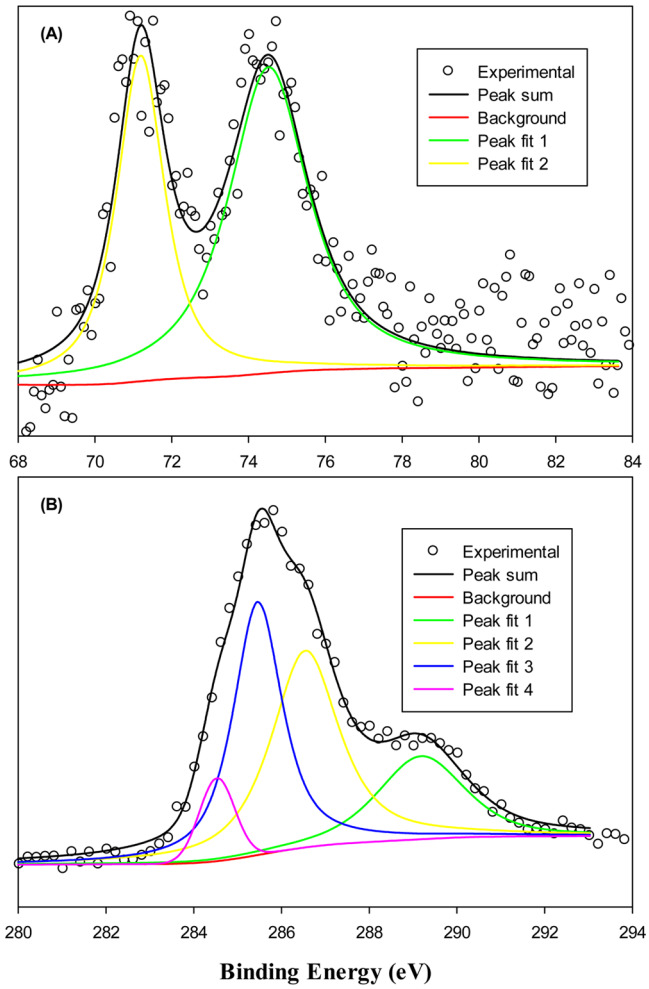

Figure 3. XPS survey spectra of the (A) Pt4f and (B) C1s electrons of the Pt/G nanoparticles. Symbols are experimental data and lines are deconvolution fits.

depicts the survey spectra of the (A) Pt4f and (B) C1s electrons of the Pt/G nanoparticles. From panel (A), the binding energies of the Pt4f electrons can be found at 71.22 and 74.63 eV. Both the doublet energies and spin−orbit coupling are consistent with those of metallic platinum.[26,27] In panel (B), deconvolution revealed four major components of the carbon 1s electrons: sp^2 C at 284.53 eV (magenta curve),[28−32] sp^3 C at 285.46 eV (blue curve),[33,34] and carbon in C−OH (286.57 eV, yellow curve) and COOH (289.20 eV, green curve) bonds.[21,35,36] This suggests the formation of various oxygenated functional moieties on the GQD surfaces. Furthermore, one may notice that the concentration of sp^2 carbons is markedly lower than those of others, likely a result of the nanoscale dimensions of the graphene quantum dots and the formation of abundant oxygenated species on the graphene surface. Such structural defects within the GQD matrix might facilitate charge transfer between platinum and adsorbed oxygen and hence lead to improved electrocatalytic performance in oxygen reduction, as detailed below.[22]

The electrocatalytic activity of the resulting Pt/G nanoparticles was then examined for oxygen reduction reactions. Figure 4 shows the steady-state cyclic voltammograms of a

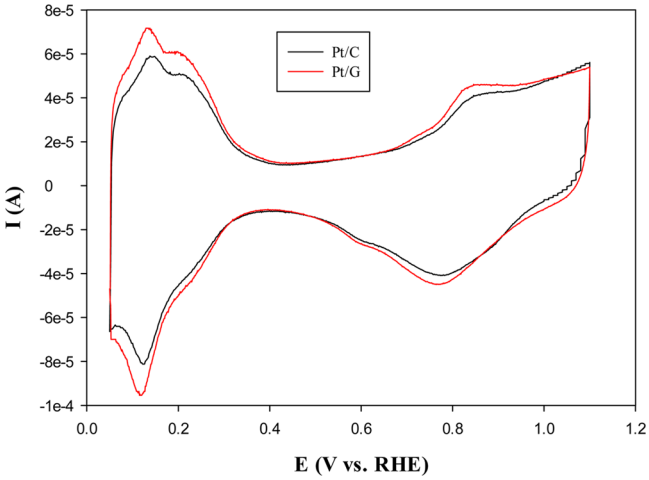

Figure 4. Cyclic voltammograms of a glassy carbon electrode (diameter 5.61 mm) loaded with Pt/G and Pt/C nanoparticle catalysts in a nitrogen-saturated 0.1 M $HClO_4$ solution. Metal loading was 12.1 μg for both nanoparticles. Potential sweep rate 20 mV/s.

glassy carbon electrode modified with a same amount of Pt/G or Pt/C in 0.1 M $HClO_4$ solution saturated with nitrogen. Both nanoparticles exhibited the well-defined butterfly voltammetric features of platinum in acid electrolytes. Of these, a pair of broad voltammetric peaks can be seen within the potential range of +0.6 and +1.0 V, which are ascribed to the formation of platinum oxide in the anodic scan and reduction of the oxide in the return sweep. Two additional pairs of voltammetric peaks appeared between 0 and +0.3 V. These are due to hydrogen adsorption/desorption on the platinum surface. Based on the integrated areas of these voltammetric features, the effective electrochemical surface area (ECSA) of the nanoparticle catalysts can be estimated to be 24.3 m^2/g for Pt/G and 20.1 m^2/g for Pt/C. In comparison to the geometric surface areas of the nanoparticles, this represents approximately 24.4% and 23.8% of the nanoparticle surface that was electrochemically accessible for the Pt/G and Pt/C nanoparticles, respectively.

The electrocatalytic activity in oxygen reduction was then examined by voltammetric measurements in an oxygen-saturated 0.1 M $HClO_4$ solution. Figure 5 shows the RRDE voltammograms of the glassy carbon disk electrode modified with (A) Pt/C or (B) Pt/G nanoparticles with the electrode rotation rate varied from 100 rpm to 2500 rpm. There are at least two aspects that warrant attention here. First, at both electrodes nonzero cathodic currents at the disk electrode (I_D) became clearly identified as the electrode potential was swept in the negative direction, and the currents increased with increasing electrode rotation rates, signifying the apparent electrocatalytic activity of both nanoparticles in oxygen reduction. Second, the corresponding ring currents (I_R) at +1.5 V were about 3 orders of magnitude lower than those of the disk, suggesting that only minimal amounts of peroxide intermediates were produced during oxygen reduction and hence high efficiency of both nanoparticles in the electrocatalytic process. In fact, the number of electron transfer (n) during oxygen reduction can be estimated by the ratio between the disk and the ring currents,[37−39]

dx.doi.org/10.1021/cs400114s | ACS Catal. 2013, 3, 831−838

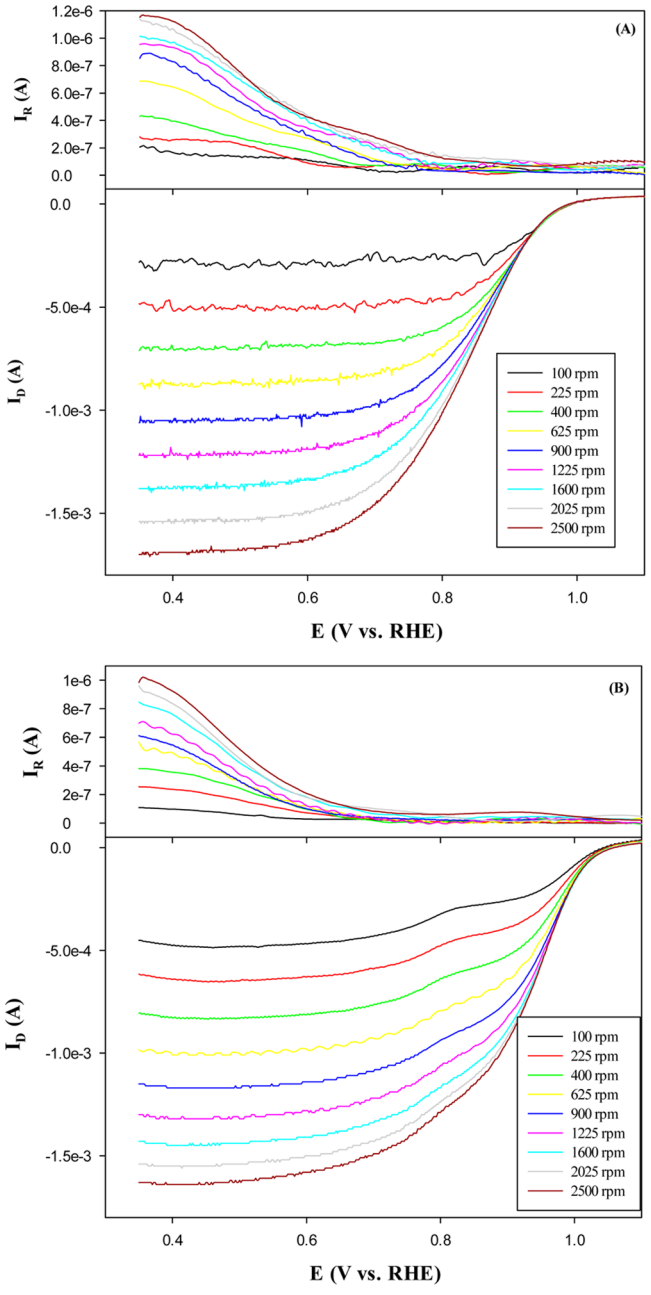

Figure 5. RRDE voltammograms of a glassy carbon electrode (diameter 5.61 mm) loaded with (A) Pt/C or (B) Pt/G nanoparticle catalysts in an oxygen-saturated 0.1 M $HClO_4$ solution. Metal loading was 12.1 μg for both nanoparticles. Potential sweep rate was 5 mV/s; electrode rotation rates were shown in the figure legends; ring potential was set at +1.5 V.

$$n = \frac{4I_D}{I_D + (I_R/N)} \quad (1)$$

where N is the collection efficiency (37%) of the RRDE electrode,[23] as depicted in Figure 6. It can be seen that at sufficiently negative potentials, both electrodes exhibited $n \approx 4.00$, indicating that oxygen was fully reduced into water, $O_2 + 4H^+ + 4e \rightarrow 2H_2O$. Yet the onset potential for oxygen reduction was markedly different. For Pt/C nanoparticles, the onset potential could be identified at +0.98 V, which was consistent with results observed previously.[23] In contrast, for Pt/G, the onset potential was substantially more positive at

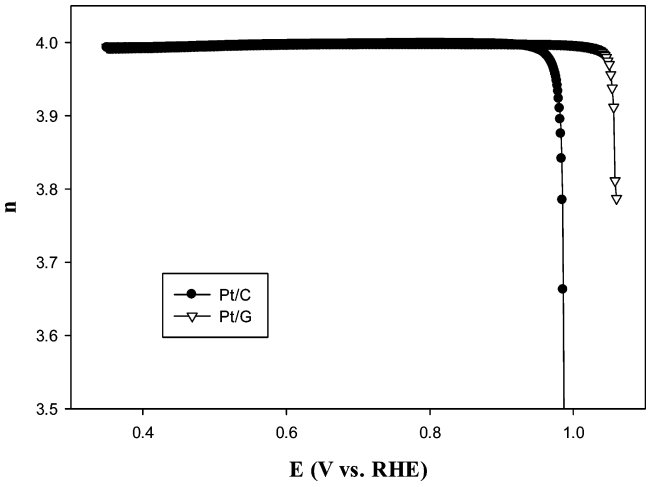

Figure 6. Variation of the number of electron transfer (n) in oxygen reduction with electrode potential. Symbols are experimental data calculated from the RRDE voltammograms at 2500 rpm in Figure 5 by using eq 1.

+1.05 V, which is among the best reported so far of oxygen reduction catalyzed by platinum nanoparticles.[12−14] Such a positive shift of about 70 mV signified the markedly improved performance of the Pt/G nanoparticles in oxygen reduction as compared to commercial Pt/C, likely a result of the electronic interactions between the platinum nanoparticles and the GQDs (more details below).

The electron-transfer kinetics involved were then quantified by the Koutecky−Levich analysis (eqs 2),[40] as the disk currents (I_D) might include both kinetic- (I_k) and diffusion (I_d)-controlled contributions,

$$\frac{1}{I_D} = \frac{1}{I_k} + \frac{1}{I_d} = \frac{1}{I_k} + \frac{1}{B\omega^{1/2}} \quad (2a)$$

$$B = 0.62nFAC_O D_O^{2/3} \nu^{-1/6} \quad (2b)$$

$$I_k = nAFkC_O \quad (2c)$$

where F is the Faradaic constant (96500 C/mol), D_O the diffusion coefficient of O_2 in 0.1 M $HClO_4$ aqueous solution (1.93×10^{-5} cm^2/s), ν the kinematic viscosity of the solution (9.87×10^{-3} cm^2/s), C_O the oxygen concentration in O_2-saturated solutions (1.18 mM), ω the electrode rotation rate, k the electron-transfer rate constant, and A the geometric surface area of the electrode.[41−43] Figure 7 depicts the Koutecky−Levich plots (I_D^{-1} vs $\omega^{-1/2}$) of both (A) Pt/C and (B) Pt/G nanoparticles within the potential range of +0.81 to +0.93 V and +0.84 to +0.99 V, respectively. First, one can see that all experimental data exhibited good linearity, and the slopes were rather consistent with each nanoparticle sample. This indicates that at both nanoparticle catalysts the oxygen reduction proceeded as a first-order reaction with respective to dissolved oxygen.

In addition, from the linear regressions in Figure 7, the kinetic currents (I_k) could also be quantified from the y-axis intercepts (eq 2c). This is manifested in the Tafel plot of Figure 7. It can be clearly seen that at both nanoparticle catalysts the kinetic currents increased with increasingly negative electrode potentials, and more importantly, within the electrode potential range of +0.80 V to +1.00 V, the kinetic currents were significantly higher with Pt/G than with Pt/C. For instance, the

dx.doi.org/10.1021/cs400114s | ACS Catal. 2013, 3, 831−838

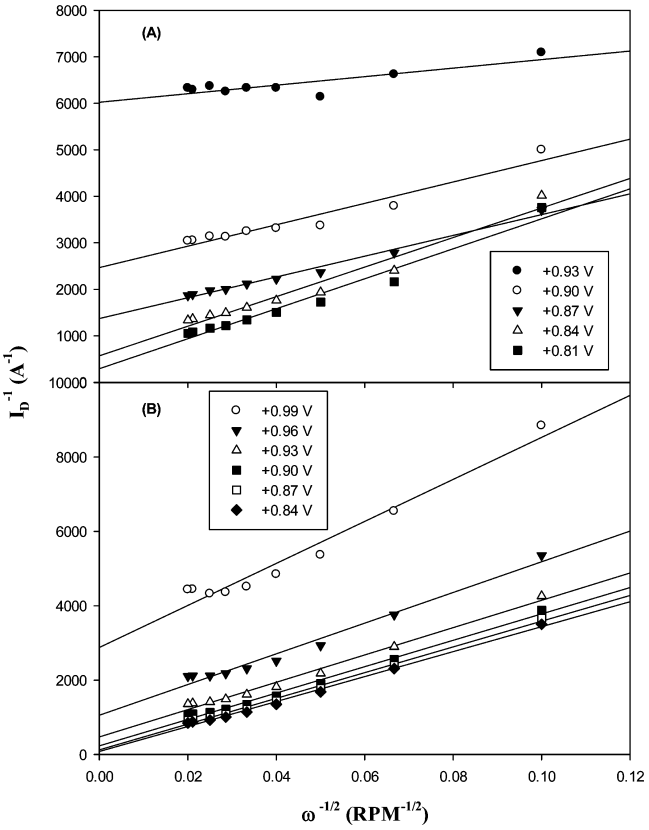

Figure 7. Koutecky–Levich plots of (A) Pt/C and (B) Pt/G nanoparticles in an oxygen-saturated 0.1 M $HClO_4$ solution. Symbols are experimental data acquired from Figure 5, and lines are the corresponding linear regressions.

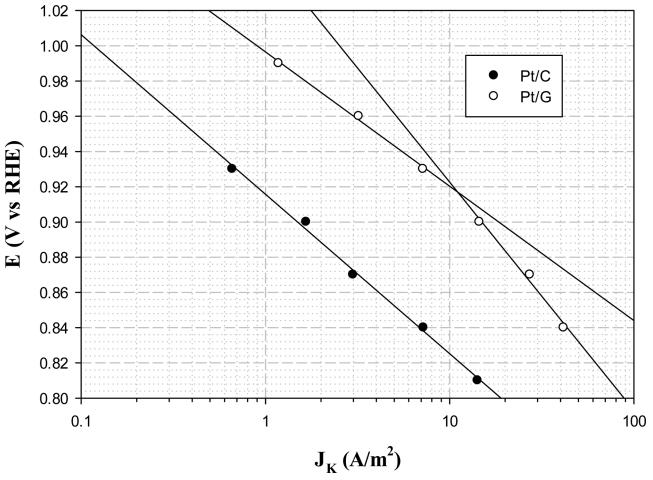

Figure 8. Variation of the kinetic current density (J_k, I_k normalized to the respective effective electrochemical surface area determined in Figure 4) with electrode potentials in oxygen reduction. Symbols are experimental data obtained from the *y*-axis intercepts of the linear regressions in Figure 7.

area-specific current density (J_k, I_k normalized by the respective effective electrochemical surface area as determined in Figure 4) at +0.90 V was 14.52 A/m^2 for Pt/G and only 1.66 A/m^2 for Pt/C. Whereas the latter is rather consistent with results obtained previously,[23,44] the former represents an almost 9 times improvement of the electrocatalytic activity, which is most likely attributable to the graphene substrate support (vide infra).

Further insights into the dynamics of oxygen reduction reactions may be obtained from the slope of the Tafel plot. Note that for oxygen electroreduction, the Tafel slopes are typically found at 60 mV/dec or 120 mV/dec, where the former corresponds to a pseudo two-electron reaction as the rate determining step, and in the latter the rate determining step is presumed to be the first-electron reduction of oxygen.[45,46] For the Pt/C nanoparticles it can be seen from Figure 8 that the Tafel slope was about 90.5 mV/dec within the potential range of +0.80 V to +0.93 V, suggesting that both processes might play an important role in the oxygen reduction reactions. In contrast, at the Pt/G nanoparticles, the Tafel plot appears to exhibit two linear segments with different slopes. At low current densities (E > +0.90 V), the Tafel slope was about 76.2 mV/dec, implying that the oxygen reduction reactions were largely limited by a pseudo two-electron process, whereas at high current densities (E < +0.90 V) the Tafel slope increased to 129.5 mV/dec, consistent with the first-electron reduction of oxygen as the rate-determining step. Such an observation of dual Tafel slopes has been observed previously,[13] and accounted for by a double-trap kinetic model,[46] where the turning point (+0.90 V in the present study) reflects the equilibrium potential for the dynamic transition between the surface-adsorbed reaction intermediates of O* and HO*. In addition, in this model, the increase of reaction rate in the low overpotential region (with a low Tafel slope) is attributed both to the decrease of the highest activation energy barrier for the forward reactions and to the increase of the lowest barrier for the backward reactions. In contrast, at large overpotentials (with a high Tafel slope), the contributions of the backward reaction diminish. Such a transition was not apparent with the commercial Pt/C, possibly because of the hydrophobic carbon black that limited the access of protons to the nanoparticle surface, whereas for Pt/G, the GQD substrates were more hydrophilic with the surface oxygenated species.

Durability is another important parameter in the quantification and comparison of nanoparticle catalytic performance. The durability test of the Pt/C and Pt/G nanoparticle catalysts was performed in oxygen-saturated 0.1 M $HClO_4$ at a potential sweep rate of 200 mV/s between +0.05 and +1.1 V for 2000 cycles. The RDE polarization curves before (black curves) and after (red curves) the tests were depicted in Figure 9. It can be seen that for the Pt/C nanoparticles (solid curves), whereas the limiting current only showed a 3% diminishment, the half-wave potential showed a cathodic shift of about 33 mV from +0.840 to +0.807 V. Markedly smaller variations were observed with the Pt/G nanoparticles (dashed curves), where the limiting current decreased by less than 2% and the shift of the half-wave potential was only 16 mV from +0.927 V to +0.911 V. These results indicate that the stability of the Pt/G nanoparticles was significantly better than that of commercial Pt/C. In fact, TEM measurements of the Pt/G nanoparticles after the durability test showed only a moderate increase (~10%) of the particle size to 3.10 ± 0.80 nm (Supporting Information, Figure S3); in contrast, in a previous study with organically capped Pt nanoparticles, the particle core size increased by almost 100% after a similar test.[23] This enhanced stability of the Pt/G nanoparticles may be ascribed to the GQD layers that wrapped around the Pt nanoparticles forming an intimate functional composite, as manifested in Figure 1.

dx.doi.org/10.1021/cs400114s | *ACS Catal.* 2013, 3, 831–838

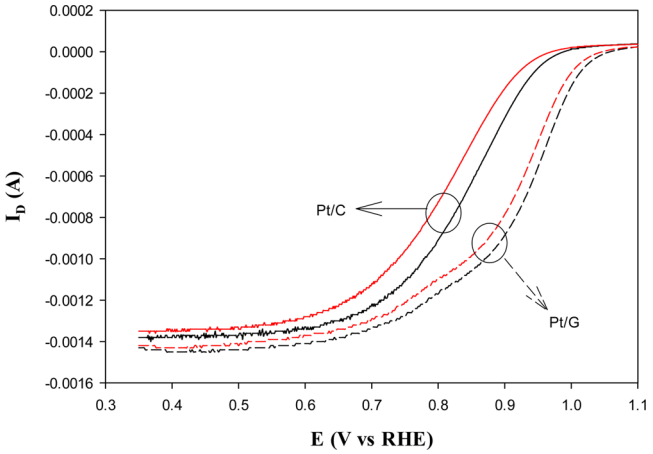

Figure 9. Polarization curves for oxygen reduction catalyzed by Pt/C (solid curves) and Pt/G (dashed curves) before (red curves) and after (red curves) 2000 potential cycles with a potential scan rate of 200 mV/s from +0.05 to +1.10 V in O_2-saturated 0.1 M $HClO_4$. Electrode rotation rate: 1600 rpm. Other experimental conditions were the same as in Figure 5.

The marked improvement of the Pt/G nanoparticles in oxygen reduction as observed above, in comparison with commercial Pt/C, might be rationalized by the impacts of the nanosized GQDs on the reaction dynamics. Note that when the O* and HO* intermediates bind strongly to the Pt surface, high overpotentials are needed in oxygen reduction. Thus, ideally a balance has to be struck between the strength of intermediate adsorption and reaction kinetics. In a recent study based on density functional theory calculations of a Pt_{13} nanoparticles supported on a monovacancy defective graphene,[22] it was found that the defective graphene support not only lowered the activation energy for oxygen (O_2) dissociation by promoting charge transfer from Pt to O_2 but also decreased the energy barrier of the rate-limiting step by weakening the binding of the HO* species. In the present study, thanks to the large surface to volume ratio, the nanosized GQDs most likely carried abundant structural detects, as manifested in the XPS measurements (Figure 3) and the appearance of apparent photoluminescence emission of the GQDs (Supporting Information, Figure S2). The intimate interactions between the graphene support and platinum nanoparticles then led to deliberate manipulation of the platinum d-band center and hence the charge transfer dynamics of oxygen reduction.[22]

CONCLUSIONS

Graphene quantum dots were prepared by chemical oxidation and exfoliation of carbon fibers and used as a unique substrate to support platinum nanoparticles by ethylene glycol thermolytic reduction of Pt(II) precursors. The composite nature of the resulting Pt/G nanoparticles (diameter 2.79 ± 0.38 nm) was examined by XRD and XPS measurements where rather substantial structural defects within the graphene quantum dots were observed. Significantly, the Pt/G nanoparticles exhibited markedly enhanced electrocatalytic activity in oxygen reduction as compared to commercial Pt/C nanoparticles. Specifically, whereas both catalysts led to full reduction of oxygen to water (i.e., n = 4), the Pt/G nanoparticles exhibited an onset potential (+1.05 V) of oxygen reduction that was about 70 mV more positive than that (+0.98 V) of commercial Pt/C nanoparticles. Furthermore, the specific activity of the Pt/G nanoparticle was almost nine times that of Pt/C, along with much improved stability. These remarkable characteristics may be ascribed to the unique support of graphene quantum dots where the structural defects led to unique manipulation of the dissociative adsorption of O_2 and the binding of reaction intermediates O* and HO* on Pt surfaces.

ASSOCIATED CONTENT

Supporting Information

Representative TEM micrograph and AFM topographic image, UV−vis and photoluminescence spectra of graphene quantum dots; TEM image of the Pt/G nanoparticles after the durability test. This material is available free of charge via the Internet at http://pubs.acs.org.

AUTHOR INFORMATION

Corresponding Author

*E-mail: shaowei@ucsc.edu.

Author Contributions

†These authors contributed equally to the work.

Notes

The authors declare no competing financial interest.

ACKNOWLEDGMENTS

This work was supported, in part, by the National Science Foundation (CHE-1012256 and CBET-1258839) and the ACS-Petroleum Research Fund (49137-ND10). TEM and XPS studies were carried out at the Molecular Foundry and National Center for Electron Microscopy, Lawrence Berkeley National Laboratory, as part of a user project.

REFERENCES

(1) Palaniselvam, T.; Irshad, A.; Unni, B.; Kurungot, S. *J. Phys. Chem. C* **2012**, *116* (28), 14754−14763.
(2) Vogel, W.; Timperman, L.; Alonso-Vante, N. *Appl. Catal., A* **2010**, *377* (1−2), 167−173.
(3) Timperman, L.; Feng, Y. J.; Vogel, W.; Alonso-Vante, N. *Electrochim. Acta* **2010**, *55* (26), 7558−7563.
(4) Liu, X.; Yao, K. X.; Meng, C. G.; Han, Y. *Dalton Trans.* **2012**, *41* (4), 1289−1296.
(5) Li, Y.; Zhu, E.; McLouth, T.; Chiu, C. Y.; Huang, X.; Huang, Y. *J. Am. Chem. Soc.* **2012**, *134* (30), 12326−12329.
(6) Zhang, K.; Yue, Q. L.; Chen, G. F.; Zhai, Y. L.; Wang, L.; Wang, H. S.; Zhao, J. S.; Liu, J. F.; Jia, J. B.; Li, H. B. *J. Phys. Chem. C* **2011**, *115* (2), 379−389.
(7) Seo, M. H.; Choi, S. M.; Kim, H. J.; Kim, W. B. *Electrochem. Commun.* **2011**, *13* (2), 182−185.
(8) Rao, C. V.; Cabrera, C. R.; Ishikawa, Y. *J. Phys. Chem. C* **2011**, *115* (44), 21963−21970.
(9) Li, Y.; Hu, Y.; Zhao, Y.; Shi, G. Q.; Deng, L. E.; Hou, Y. B.; Qu, L. T. *Adv. Mater.* **2011**, *23* (6), 776.
(10) Li, Y.; Zhao, Y.; Cheng, H.; Hu, Y.; Shi, G.; Dai, L.; Qu, L. *J. Am. Chem. Soc.* **2012**, *134* (1), 15−18.
(11) Zhang, Z. P.; Zhang, J.; Chen, N.; Qu, L. T. *Energy Environ. Sci.* **2012**, *5* (10), 8869−8890.
(12) He, D. P.; Cheng, K.; Peng, T.; Sun, X. L.; Pan, M.; Mu, S. C. *J. Mater. Chem.* **2012**, *22* (39), 21298−21304.
(13) Vinayan, B. P.; Nagar, R.; Ramaprabhu, S. *J. Mater. Chem.* **2012**, *22* (48), 25325−25334.
(14) Tan, Y. M.; Xu, C. F.; Chen, G. X.; Zheng, N. F.; Xie, Q. J. *Energy Environ. Sci.* **2012**, *5* (5), 6923−6927.
(15) Park, S.; Ruoff, R. S. *Nat. Nanotechnol.* **2009**, *4* (4), 217−224.
(16) Huang, X.; Zeng, Z. Y.; Fan, Z. X.; Liu, J. Q.; Zhang, H. *Adv. Mater.* **2012**, *24* (45), 5979−6004.

(17) Huang, C. C.; Li, C.; Shi, G. Q. *Energy Environ. Sci.* **2012**, *5* (10), 8848−8868.
(18) Cote, L. J.; Kim, J.; Tung, V. C.; Luo, J. Y.; Kim, F.; Huang, J. X. *Pure Appl. Chem.* **2011**, *83* (1), 95−110.
(19) He, D.; Cheng, K.; Li, H.; Peng, T.; Xu, F.; Mu, S.; Pan, M. *Langmuir* **2012**, *28* (8), 3979−3986.
(20) Shen, J. H.; Zhu, Y. H.; Yang, X. L.; Li, C. Z. *Chem. Commun.* **2012**, *48* (31), 3686−3699.
(21) Peng, J.; Gao, W.; Gupta, B. K.; Liu, Z.; Romero-Aburto, R.; Ge, L. H.; Song, L.; Alemany, L. B.; Zhan, X. B.; Gao, G. H.; Vithayathil, S. A.; Kaipparettu, B. A.; Marti, A. A.; Hayashi, T.; Zhu, J. J.; Ajayan, P. M. *Nano Lett.* **2012**, *12* (2), 844−849.
(22) Lim, D. H.; Wilcox, J. *J. Phys. Chem. C* **2012**, *116* (5), 3653−3660.
(23) Zhou, Z. Y.; Kang, X. W.; Song, Y.; Chen, S. W. *Chem. Commun.* **2012**, *48* (28), 3391−3393.
(24) Gloaguen, F.; Andolfatto, F.; Durand, R.; Ozil, P. *J. Appl. Electrochem.* **1994**, *24* (9), 863−869.
(25) Kang, X. W.; Chen, S. W. *J. Mater. Sci.* **2010**, *45* (10), 2696−2702.
(26) Wagner, C. D.; Muilenberg, G. E., *Handbook of x-ray photoelectron spectroscopy: a reference book of standard data for use in x-ray photoelectron spectroscopy*; Perkin-Elmer Corp., Physical Electronics Division: Eden Prairie, MN, 1979; p 190.
(27) Dablemont, C.; Lang, P.; Mangeney, C.; Piquemal, J. Y.; Petkov, V.; Herbst, F.; Viau, G. *Langmuir* **2008**, *24* (11), 5832−5841.
(28) Rybachuk, M.; Bell, J. M. *Carbon* **2009**, *47* (10), 2481−2490.
(29) Turgeon, S.; Paynter, R. W. *Thin Solid Films* **2001**, *394* (1−2), 44−48.
(30) Dettlaff-Weglikowska, U.; Benoit, J. M.; Chiu, P. W.; Graupner, R.; Lebedkin, S.; Roth, S. *Curr. Appl. Phys.* **2002**, *2* (6), 497−501.
(31) Iucci, G.; Carravetta, V.; Altamura, P.; Russo, M. V.; Paolucci, G.; Goldoni, A.; Polzonetti, G. *Chem. Phys.* **2004**, *302* (1−3), 43−52.
(32) Siegbahn, K. *Philos. Trans. R. Soc. S-A* **1970**, *268* (1184), 33.
(33) Zhang, S.; Chandra, K. L.; Gorman, C. B. *J. Am. Chem. Soc.* **2007**, *129* (16), 4876.
(34) Okpalugo, T. I. T.; Papakonstantinou, P.; Murphy, H.; McLaughlin, J.; Brown, N. M. D. *Carbon* **2005**, *43* (1), 153−161.
(35) Bajpai, R.; Roy, S.; Kulshrestha, N.; Rafiee, J.; Koratkar, N.; Misra, D. S. *Nanoscale* **2012**, *4* (3), 926−930.
(36) Moon, I. K.; Lee, J.; Ruoff, R. S.; Lee, H. *Nat. Commun.* **2010**, *1*, 73−81.
(37) Lefèvre, M.; Dodelet, J.-P. *Electrochim. Acta* **2003**, *48* (19), 2749−2760.
(38) Gojković, S. L.; Gupta, S.; Savinell, R. F. *Electrochim. Acta* **1999**, *45*, 889−897.
(39) Meng, H.; Larouche, N.; Lefèvre, M.; Jaouen, F.; Stansfield, B.; Dodelet, J.-P. *Electrochim. Acta* **2010**, *55* (22), 6450−6461.
(40) Lim, B.; Jiang, M.; Camargo, P. H.; Cho, E. C.; Tao, J.; Lu, X.; Zhu, Y.; Xia, Y. *Science* **2009**, *324* (5932), 1302−1305.
(41) Schumpe, A.; Adler, I.; Deckwer, W. D. *Biotechnol. Bioeng.* **1978**, *20* (1), 145−150.
(42) Anastasijevic, N. A.; Dimitrijevic, Z. M.; Adzic, R. R. *Electrochim. Acta* **1986**, *31* (9), 1125−1130.
(43) Markovic, N. M.; Gasteiger, H. A.; Grgur, B. N.; Ross, P. N. *J. Electroanal. Chem.* **1999**, *467* (1−2), 157−163.
(44) Zhou, Z.-Y.; Kang, X. W.; Song, Y.; Chen, S. W. *J. Phys. Chem. C* **2012**, *116* (19), 10592−10598.
(45) Zhang, J. *PEM fuel cell electrocatalysts and catalyst layers: fundamentals and applications*; Springer: London, 2008.
(46) Wang, J. X.; Uribe, F. A.; Springer, T. E.; Zhang, J. L.; Adzic, R. R. *Faraday Discuss.* **2008**, *140*, 347−362.